MeatSpec: Enabling Ubiquitous Meat Fraud Inspection through Consumer-Level Spectral Imaging

Haiyan Hu[1], Yinan Zhu[1], Baichen Yang[1], Hua Kang[2], Shanwen Chen[1], Qian Zhang[1]*

[1]Department of Computer Science and Engineering, The Hong Kong University of Science and Technology
[2]Noah's Ark Lab, HUAWEI

ABSTRACT

Meat adulteration is a significant problem that can pose health risks economic losses to consumers. Current detection methods are hindered by high costs, limited capabilities, or time-consuming sample preparation, making them only accessible in laboratory tests and can not protect the safety of end-users. This paper introduces MeatSpec, a low-cost and user-friendly system for detecting meat adulteration using spectral imaging, to move the adulteration inspection out of laboratories. MeatSpec employs a multispectral camera to reduce costs while quickly capturing spectral images, but this leads to a decrease in spectral resolution and coverage. To solve this challenge, the system uses spectral reconstruction technology and innovative designs tailored for meat adulteration detection. This includes involving adulteration-related prior information during the reconstruction training phase and incorporating contrastive learning to enlarge the distances among reconstructed samples belonging to various adulteration types. Additionally, we devise distinct feature extractors for different bands based on characteristics of the reconstructed spectra and employ knowledge distillation to mitigate error in full-band reconstructed spectra while capturing features related to adulteration. Experimental evaluations on 347 paired spectral images demonstrate that our system achieves a 91.06% accuracy in detecting multiple adulteration types, merely 7.78% inferior to the expensive professional solution, yet 21.58% superior to the baseline at the same price point.

---

*The corresponding author is Qian Zhang (qianzh@cse.ust.hk).

CCS CONCEPTS

• **Computing methodologies → Machine learning**; • **Human-centered computing → Ubiquitous and mobile devices**.

KEYWORDS

Meat Adulteration, Spectral Imaging and Reconstruction

1 INTRODUCTION

Meat adulteration is a growing concern with significant health and economic implications. The practice of adulterating meat products involves substituting animal-derived ingredients, injecting water, and using illegal additives [5], which can cause health risks such as foodborne illnesses, allergic reactions, cancer, and kidney damage [6, 19, 35]. Additionally, reports show end-of-chain nodes, like catering and retail, are the most vulnerable victims of food fraud [46], which is in-demanding for adulteration detection solutions that are cost-effective, convenient, and without professional operations.

However, existing solutions can not meet this requirement. High requirements for detection capabilities are required due to the notable similarity in composition between adulterated and unadulterated meat samples [1]. Most methods encounter difficulty in achieving a balance between the high detection capability and reasonable cost of the system. Standard detection methods [33, 34, 36] are expensive and require specialized laboratory settings. Hyperspectral solutions [20, 21], while capable of obtaining accurate results without sample preparation, require complex and expensive equipment (costing over $10,000). Conversely, some low-cost solutions like electronic noses [25] or image classification [38, 43] exhibit limited detection capabilities to discern

in-depth chemical characteristics, may miss the most harmful adulteration problem, *e.g.*, veterinary drugs or antibiotic residues. Currently, there is no consumer-grade system that can detect various meat adulteration.

In this paper, we try to bridge the gap by developing a low-cost and user-friendly system for ubiquitous meat adulteration inspection based on spectral imaging. By minimizing the cost, our system can be deployed in ubiquitous dining scenarios, including schools, catering outlets, or halal households to help users quickly get meat adulteration inspection without professional experience. To accomplish this, we first choose an off-the-shelf low-cost multispectral camera [44], which costs one hundredth of a fine-grained hyperspectral camera, as the hardware equipment to significantly minimize the system expenses. Nevertheless, the decrease in hardware cost leads to a decline in both spectral resolution and spectral coverage range, both of which are essential for efficient meat adulteration detection. Fortunately, we are inspired by the fact that spectral reconstruction (SR) technology can recover fine-grained spectral resolution and extend spectral covering range of limited spectral measurements, such as RGB or multispectral images [4, 27, 41, 49, 51]. This technology presents an opportunity to extend the capability of a low-cost multispectral camera to meet the requirements for ubiquitous meat adulteration detection.

However, applying spectral reconstruction algorithms to develop a low-cost meat adulteration detection system is not a trivial task. It faces the following challenges: **(1) High Similarity of Multispectral Images.** The resemblance between authentic and adulterated samples, especially those with low adulterant concentration, yields analogous spectral attributes, complicating adulteration detection. The low-cost multispectral camera worsens the problem due to its coarse-grained spectral resolution. However, existing spectral reconstruction algorithms cannot reconstruct distinguishable results between two samples sharing similar or even the same multispectral characteristics. **(2) Full-Band Reconstruction Error.** Since the spectral absorption characteristics of different adulteration types span across diverse wavelengths, it is essential for the system to cover a sufficiently broad spectral range, usually 400-1000nm [20, 21]. However, no low-cost multispectral devices can cover such a wide wavelength range. When applying existing spectral reconstruction algorithm for full-band (*i.e.*, 400-1000nm) reconstruction, the errors and noises in reconstructed data will hinder its usability for adulteration detection. **(3) Lack Spectral Reconstruction Dataset.** Spectral reconstruction algorithms require paired (multispectral images, hyperspectral images) data for training. However, obtaining exactly the paired data is challenging. As the field-of-view (FOV) and focal length of the spectral cameras are different, to cover the same scene, the system should be used at a specific fixed distance and angle, which is impractical to implement physically. Previous methods use opened hyperspectral images (HSI) dataset and subsampled HSI as paired multispectral images (MSI) for training, but this approach can result in different distributions of training and test data, leading to reduced performance during deployment.

To overcome the above challenges, we present MeatSpec, the first consumer-grade spectral imaging system for ubiquitous meat adulteration inspection. Specifically, MeatSpec can distinguish between six common types of adulteration, such as substitution, veterinary drug residues, and additives, and use one of the most common targets in meat adulteration cases, *i.e.*, beef, as authentic samples [28]. MeatSpec solves the above challenges with the following designs. **Firstly**, we propose an application-oriented spectral reconstruction (AOSR) module to restore more distinguishable reconstructed images for the cost-effective multispectral input. Specifically, AOSR involves adulteration related prior information during the SR training phase and incorporates contrastive learning that enlarges the distances among reconstructed samples belonging to various adulteration types (see § 3.1). **Secondly**, to suppress noise and error in full-band reconstructed spectra and extract adulteration-related features, MeatSpec proposes a reconstruction-adapted adulteration detection (RAAD) module. RAAD designs distinct feature extractors for different bands according to the error distribution characteristics of the reconstructed spectra, and employs knowledge distillation to align extracted features with the original HSI's features in the latent feature space (see § 3.2). **Thirdly**, we collect a dataset comprising 347 paired reconstruction training data through our designed pre-processing pipeline. The pipeline involves several steps to ensure that the MSI and HSI data are aligned and addresses challenges posed by ambient light influence, resolution differences, and variations in sample location during data collection (see § 3.3).

We implement a fully-functional prototype of MeatSpec at a cost of less than $60. We demonstrate the system's capability in detecting minced beef adulteration. Six common types of adulteration, namely substitution, dye substitution, low-quality meat, water injection, edible additives, and toxic additives are considered. For each type of adulteration, we select various typical adulterants, resulting in a total of 13 different adulterants. Results show MeatSpec achieves a 91.06% accuracy in detecting multiple adulteration types, merely 7.78% inferior to the expensive professional solution, yet 21.58% superior to the baseline at the same price point, demonstrating the effectiveness of the system design. We also verify that MeatSpec is robust to various environmental setups, such as meat size, placement, and ambient illumination.

In summary, we make the following contributions:

- We develop MeatSpec, the first consumer-grade meat adulteration detection system that can accurately distinguish authentic meat and identify the types of adulteration.
- We propose a novel spectral reconstruction scheme and a classification model that fit the reconstructed spectral images, enhancing the accuracy and reliability of meat adulteration detection.
- We open the dataset [31] of beef adulteration detection with 347 paired HSI and MSI data for 13 different adulterants and design a pipeline for aligning spectral reconstruction training data.
- Experimental results demonstrate MeatSpec's high accuracy in detecting various adulteration types and robustness under various experimental and environmental setups.

2 BACKGROUND AND CHALLENGES

2.1 Background

2.1.1 Meat Adulteration Detection with Spectroscopy. Spectroscopy is a valuable technique for analyzing various properties of substances, including composition, structure, and concentration [47]. In the context of meat adulteration, the chemical profile, such as fatty acid and myoglobin, of each meat species is unique, varying in type and quantity across different tissues [9, 20, 21].

Figure 1 illustrates two typical spectral imaging system, *i.e.*, HSI and MSI, scanning the same meat sample. In principle, a spectral image can be formulated as:

$$I_c(x, y, w) = R(x, y, w)E_c(w)S_c(w), \qquad (1)$$

where $R(x, y, w)$ is the spectral reflectance of the object, x, y and w are the width, height and wavelength channel respectively. The spectral reflectance is the key attribute for identifying substances. $E_c(w)$ is the illumination spectrum, and $S_c(w)$ denotes the spectral response function, both determined by the hardware parameters of the spectrum acquisition system. Typically, the MSI systems tend to cover small range and have few number of filters than HSI systems due to the cost and size limitation [39, 44]. In contrast, hyperspectral imaging devices are always too expensive, costing over $10,000, limiting their accessibility to the majority of users [12].

2.1.2 Spectral Reconstruction. Spectral reconstruction (SR) aims to recover the hyperspectral image (HSI) using a reduced set of measurements or observations, such as MSI, RGB images, or compressed hyperspectral data. The rationale behind hyperspectral reconstruction is based on three key characteristics.

- *Inherent Redundancy.* Neighboring spectral bands in HSI often exhibit high correlation, allowing for leveraging information from adjacent bands to estimate the spectral content of missing or unobserved bands.
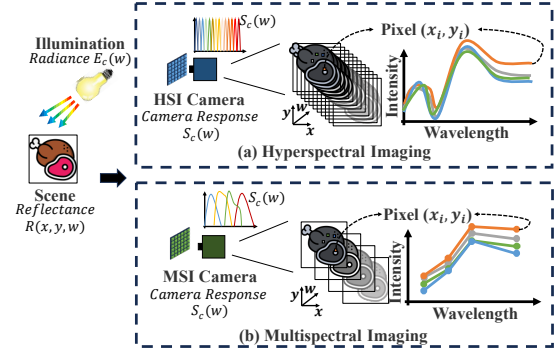

Figure 1: Various spectral imaging processes of the same meat sample.

- *Sparsity.* HSI tends to demonstrate sparsity in both the spectral and spatial domains, allowing for exploiting this sparsity to reconstruct the full hyperspectral image from a reduced set of measurements.
- *Spectral Mixing.* HSI can be represented as a linear or nonlinear combination of a limited number of spectral signatures, further facilitating the reconstruction process.

In this way, we can offer a promising solution to overcome the cost barrier associated with acquiring HSI for meat adulteration detection. Currently, lots of deep learning reconstruction algorithms have been proposed and shown good performance in RGB image reconstruction tasks [2, 4, 13, 27].

2.2 Challenges

However, the application of these state-of-the-art (SOTA) SR algorithms for meat adulteration detection may face challenges when it comes to reconstructing accurate spectra for similar substances. We conduct comparison experiments using a SOTA spectral reconstruction algorithm, named AWAN [27] to illustrate the problems.

(1) High Similarity of Multispectral Images. As we mentioned before, the similarity in composition (*e.g.*, fatty and myoglobin) between adulterated and authentic meat samples is the main challenge in the detection of meat adulteration [1]. The use of low-cost multispectral cameras exacerbates the challenge. As shown in Figure 2, when using a low-cost multispectral device to capture spectral images of similar samples $C1$ and $C2$, the camera can only capture a limited number of spectral bands, resulting in coarse-grained spectra lacking detailed information. Within these limited spectral bands, the MSI spectra of authentic meat and adulterated samples may look further similar or even identical.

Unfortunately, previous SR algorithms can not solve this problem. The rationale of the spectral reconstruction is to learn a one-to-one mapping from paired (MSI, HSI) for the same scene. Therefore, for two different HSIs sharing similar or even the same MSI, the SR algorithm can hardly restore the subtle differences present in the original HSIs, making
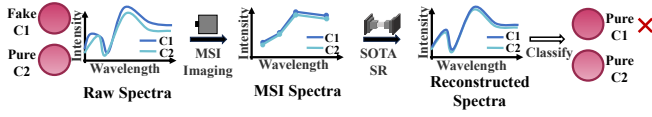
Figure 2: Illustration of how low-cost MSI imaging MSI imaging makes it harder to tell similar samples apart.

Table 1: Comparison of the cross-type variances (Euclidean distances) among raw spectra, MSI spectra, and reconstructed spectra using SOTA SR.

Data	Cross-type Variances
Raw Spectra	0.1951
MSI Spectra	0.1805
Recon (SOTA)	0.1764
MeatSpec	0.2311

the reconstructed spectra difficult to distinguish between adulterated and authentic meat. Table 1 shows the Euclidean distances between different adulteration classes of original HSIs, cost-effective MSIs, and reconstructed data from SOTA SR algorithm in our meat adulteration dataset [31]. We can find that low-cost MSI imaging and the existing SR algorithm both narrow the distance between different types of adulterated samples.

(2) Full-Band Reconstruction Error. Since the spectral absorption characteristics of different adulteration types span across diverse wavelengths, it is essential for the system to cover a sufficiently broad spectral range, *i.e.*, 400-1000nm. Thus, we conduct full-band spectral reconstruction and utilize the reconstructed HSI data for adulteration detection. However, most previous models for meat adulteration detection utilize the pure HSI data as input [21, 23], rather than constructed HSI. Accordingly, these models do not consider the following characteristics of reconstructed HSI data. First, due to the reconstruction error, reconstructed HSI exists more spectral-spatial noises and useless information than pure HSI. Second, since our MSI data does not cover the visible band, it's hard to accurately reconstruct hyperspectral images in the visible band (see Figure 3(a)). These errors and noises in the reconstructed data will hinder its usability for adulteration detection. Thus, previous models cannot directly adapt to our reconstructed HSI data and will perform bad. Moreover, we observe that the reconstructed spectra has large cross-type variances inside the visible band (see Figure 3(b)), which differs from the original HSI.

(3) Lack Spectral Reconstruction Dataset. In principle, the spectral reconstruction algorithm needs to obtain paired MSIs and HSIs under the same scene, *i.e.*, having the same $R(x, y, w)$. However, obtaining exactly the same $R(x, y, w)$ using the two systems is challenging. As the field-of-view (FOV) and focal length of the two systems are different, to
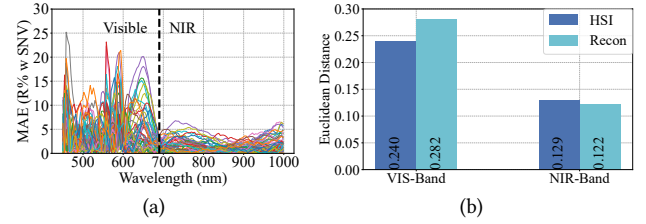

Figure 3: (a) Reconstruction error of average spectra after SNV. Each color corresponds to one sample. (b) Comparison of the cross-type variances between the original HSI and reconstructed HSI in the visible and near infrared bands.

Table 2: Comparison of reconstruction error between simulated MSI and real MSI using model trained on simulated MSI data.

Data	RMSE	MRAE
Simulated Test MSI	0.0095	0.0234
Real Test MSI	106.71	268.52

cover the same scene, the system should be used at a specific fixed distance and angle, which is impractical to implement physically. The previous reconstruction works utilizes known response curves of RGB cameras to simulate training RGB data from HSI [27, 40]. However, there is no open response curves library of MSI devices and we can not access the response curve of an off-the-shelf MSI device. We simulate several response curves using Gaussian distribution refers to [48]. However, simulation can not restore the MSI data acquisition process, such as MSI detector response, dark current noise, *etc.*, resulting in different distribution of training data and test data. As shown in Table 2, model training on simulated data significantly reduce reconstruction performance during actual deployment.

3 SYSTEM DESIGN

Figure 4 shows the architecture of our system. The goal of MeatSpec is to extract useful information from low-quality data for accurate meat adulteration detection. To achieve this, MeatSpec incorporates two modules: application-oriented spectral reconstruction (AOSR in § 3.1) and reconstruction adapted adulteration detection (RAAD in § 3.2) to process the data collected from cost-effective MSI hardware. In addition, we design a novel pipeline to align paired (MSI, HSI) data for model training and collect a dataset comprising 347 paired spectral reconstruction training data (see § 3.3).

3.1 Application-Oriented Spectral Reconstruction

To address the challenge of high similarity, we need to modify the existing SR algorithm to enable it to capture the subtle differences among similar MSI spectra of different meat
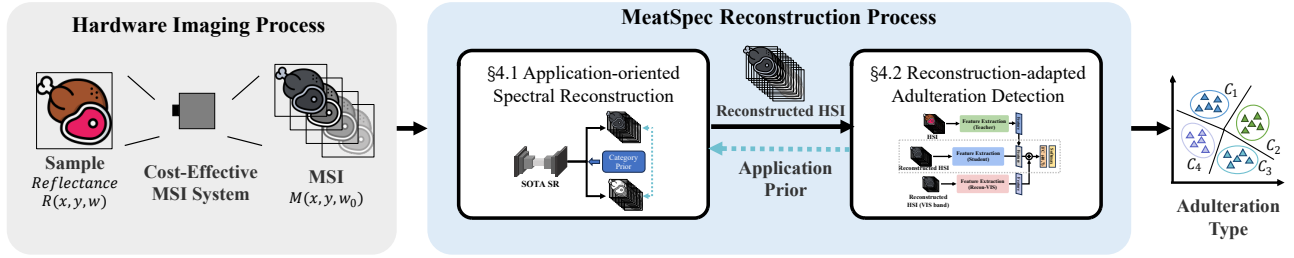
Figure 4: The system structure of MeatSpec, which consists of two parts: application-oriented spectral reconstruction (AOSR § 3.1) and reconstruction-adapted adulteration detection (RAAD § 3.2).

categories. To this end, MeatSpec proposes an application-oriented spectral reconstruction model, which introduces application related prior information during the training phase and incorporates contrastive learning to enlarge the distances among reconstructed samples that share similar MSIs inputs. By this approach, the reconstructed spectra can be better discriminated among different categories of meat samples, enhancing the accuracy and reliability of meat adulteration detection. Figure 5 illustrates the structure of our proposed AOSR model. As we can see, the objective of the model consists of two parts: $\mathscr{L}_h$ is the reconstruction loss between the reconstructed spectra and ground truth spectra for the same sample, and $\mathscr{L}_c$ denotes the contrastive loss of the reconstructed spectra among different categories. Two losses are weighted by α to adjust the balance between different learning objectives.

Base Reconstruction Model. We first leverage a SOTA spectral reconstruction algorithm [27] as the backbone of our AOSR model to reconstruct the hyperspectral image $\hat{R}(x, y, w)$ for the MSI input $M(x, y, w_0)$. The purpose of using SR backbone is two-fold, increasing the spectral resolution and extending the spectral coverage. Therefore, $\hat{R}(x, y, w)$ will have a wider covering range and more number of bands than $M(x, y, w_0)$ to support meat adulteration detection. We make some simple modifications on [27] to fit our MSI reconstruction task. Firstly, as [27] takes RGB images instead of MSI as input, we modify its input and output size to fit our dataset. Then, since we utilize an off-the-shelf MSI camera, which can not access its camera spectral sensitivity (CSS) parameters, we remove the CSS loss in [27]. After modification, the reconstruction loss of our base model is defined as:

$$\mathscr{L}_h = \frac{1}{M} \sum_{i=1}^{M} \frac{|\hat{R}^i - R^i|}{R^i}, \quad (2)$$

where M is the total number of pixels, $\hat{R}^i$ and R^i denote the reconstructed and original spectrum of the i-th pixel for the sample. By minimizing the loss $\mathscr{L}_h$, the model can narrow the distance between the reconstructed HSI and real HSI.

Contrast-based Reconstruction. We then introduce meat adulteration prior information and exploit contrastive learning into the training phases. Our goal is to enable the
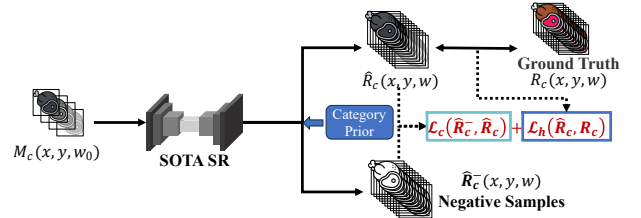

Figure 5: The working process of application-oriented spectral reconstruction model.

model to distinguish between different classes of samples that share similar or the same multispectral features. In light of this, we construct contrastive loss that maximizes the distance of reconstructed HSI among different categories. We use Euclidean distance to measure the distance of the reconstructed HSI between two samples. We then use the introduced adulteration prior information to screen negative samples for each sample. The negative samples are defined as the samples from the categories that are different from the target within one batch. Our contrastive loss is calculated as follows:

$$\mathscr{L}_c = -\frac{1}{B} \sum_{b^-=1, b^- \neq b}^{B} \mathbb{1}(y_b \neq y_{b^-}) \sqrt{\frac{1}{M} \sum_{i=1}^{M} \|\hat{R}_b^i - \hat{R}_{b^-}^i\|^2}, \quad (3)$$

where B is the batch size. $\hat{R}_b^i$ and $\hat{R}_{b^-}^i$ are the i-th reconstructed pixel of sample b and sample b^-. y_b and y_{b^-} are the category label of sample b and b^-. The function indicates that we only maximize the distance between the target sample b and the others having different categories within the batch. As a result, contrastive learning enables the reconstruction algorithm to have better distinguishing capability. As depicted in Table 1, by using our design, the distances between different adulteration classes of reconstructed HSIs improve from 0.1764 to 0.2311. Further evaluation of the effectiveness of our designed AOSR module is discussed in § 5.3.1.

3.2 Reconstruction-adapted Adulteration Detection

3.2.1 Reconstruction Data Refinement. To combat the noise and redundant information induced during spectral reconstruction, we consider to refine the reconstructed data as

follows. First, we divide each reconstructed hyperspectral image into 40×40 patches and conduct average pooling on each patch to reduce the spatial-wise redundant information and accelerate the training process. Next, for spectral-wise denoising, we utilize a mean filter with a window size of 3 to smooth the spectra at each pixel. Then, we apply the common spectral preprocessing method namely standard normalized variate (SNV) on each pixel's spectra to reduce the scattering effect. After these operations, each processed HSI cube with 40×40 pixels and 138 channels will be inputted into our designed CNN classifier below.

3.2.2 Reconstruction-adapted CNN Model. As shown in Figure 6, our adulteration detection model contains three parts: base model, feature distillation and visible information extraction, based on the characteristics of reconstructed data.

Base Model Design. Our base model leverages the refined HSI data (40×40×138) as input, which adopts three 2D convolutional layers, three batch normalization (BN) layers, three pooling layers and one fully connected (FC) layer. Considering the large noise of reconstructed HSI, the first convolution layer conducts down-sampling to reduce the effect of noise and redundant information. Meanwhile, it does not reduce the spectral-wise dimension, which instead assigns each channel a weight for better feature extraction. Besides, to further avoid overfitting by reconstruction noise, a BN layer and maximum pooling are added after the first convolutional layer. These three layers act as a special denoising module for reconstructed HSI. Then, the output will be inputted to the second convolution layer where we leverage a larger kernel size to extract more global information, because the reconstructed spatial texture may contain incorrect noise and lead to overfitting. So we pay more attention to the global information and spectral dimension. The third convolution layer has the same setting as the second one, which further extracts more fine-grained features. After average pooling to remove the spatial dimension, we can obtain a 32-length embedding, denoted by F_s.

Feature Distillation. As shown in Figure 3(a), it's hard to accurately reconstruct the visible band. But, since the spectral absorption characteristics of different adulteration types are distributed in different bands, we need to utilize the full-band information of the original HSI for effective adulteration detection. To achieve this, we decide to exploit the feature distillation approach. By guiding the feature extractor of reconstructed HSI with that of original HSI, we can transfer the useful knowledge of full band, especially the visible band, for better adulteration detection. Specifically, we regard the base model as the student model and add a branch of teacher model with the original HSI as input. Since the original HSI has little noise, we can reduce its spatial dimension to 20×20 pixels after SNV to further accelerate
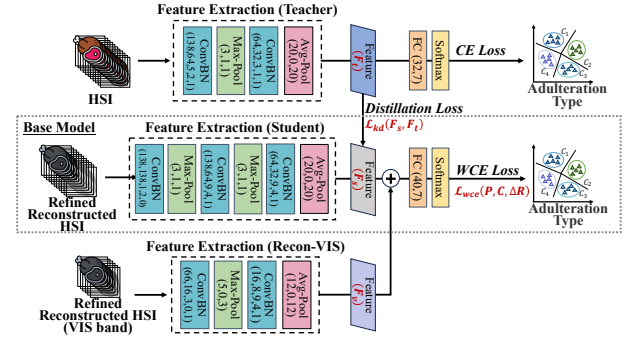

Figure 6: Model design of reconstruction-adapted adulteration detection.

the training. Meanwhile, the teacher model only needs to use two convolutional layers with smaller kernel sizes than that of the student model, and the corresponding BN layers and pooling layers. After training the teacher model, we freeze its model parameters and extract the 32-length embedding before FC layer as the teacher feature, denoted by F_t. Then, we minimize the gap between the extracted features of the student model (F_s) and the frozen teacher model (F_t) for feature distillation.

Visible Information Aid. Though the visible band is hard to reconstruct, contrastive learning itself can bring some new information inside the reconstructed visible band, due to the usage of negative samples. Figure 3(b) demonstrates that the reconstructed visible band has more information to distinguish diverse categories than the original visible band. This additional information may help enhance the classification performance. Therefore, we add a branch in our model to extract the additional feature inside the visible band of reconstructed HSI (*i.e.*, the first 66 channels). We extract an 8-length embedding, demoted by F_v, and concatenate it with our distilled feature. Finally, a formed 40-length feature is fed to the FC layer for classification.

Weighted Loss. Eventually, the overall loss function for our CNN model consists of a distillation loss $\mathscr{L}_{kd}$ and a weighted cross-entropy (WCE) loss $\mathscr{L}_{wce}$ as:

$$\mathscr{L} = \beta \cdot \mathscr{L}_{kd} + (1-\beta) \cdot \mathscr{L}_{wce} \qquad (4)$$

where β is the weight to trade off the strength of feature distillation for different objects. Note that we define a novel weighted cross-entropy loss for our classification task. We observe that different adulteration types have different degrees of reconstruction error. Larger errors may cause greater difficulty to distinguish. Therefore, we compute the average reconstruction error of each adulteration type as its class weight, which is used in cross-entropy loss for better classification performance:

$$\mathscr{L}_{wce} = -\log(P_c)\frac{1}{N_c}\sum_{i=1}^{N_c}\Delta R_i \qquad (5)$$

Table 3: Adulterants and their concentrations in our collected dataset. Six common types of adulteration and 13 different adulterants with each containing two concentrations are considered.

Types	Adulterants	Concentration
Substitute	Pork	10%, 50%
	Chicken	10%, 50%
	Duck	10%, 50%
Dye Substitute (Color & Essence)	Pork	10%, 50%
	Chicken	10%, 50%
	Duck	10%, 50%
Low Quality	Beef Offal	10%, 50%
	Stale Beef	10%, 50%
Edible Additive	Vegetable Protein	5%, 20%
Water Injected	Water	5%, 20%
Toxic Additive	Antibiotic	(0.75, 3) ug/kg
	Stimulant	(0.3, 1.2) ug/kg
	Preservative	(0.15, 0.6) mg/kg

where N_c denotes the sample number of the c-th adulteration type, ΔR_i denotes the average reconstruction error of i-th sample and P_c denotes the classification probability to c-th class. In this way, the classification model will pay more attention to those classes with poor reconstruction performance. Besides, for the feature distillation, we use MSE loss as the distillation loss to measure the gap distance between the extracted student features and teacher feature, *i.e.*, $\mathcal{L}_{kd} = \frac{1}{N_F}||F_t - F_s||^2$, where N_F is 32. The distillation loss is jointly used with cross-entropy loss during training, which ensures the distillation trend towards high classification accuracy. The effectiveness of our designed RAAD module is evaluated in § 5.3.2.

3.3 Meat Spectral Reconstruction Dataset Development

To achieve an effective data alignment, we design a pre-processing pipeline through image processing algorithms. The pipeline involves four steps to ensure that the MSI and HSI data are aligned and addresses challenges posed by ambient light influence, resolution differences, and variations in sample location during data collection. **(1) Elimination of Ambient Light.** In real-world scenarios, the uncontrollable intensity of environmental illumination may hinder learning a reliable reconstruction mapping. To overcome this, we apply background subtraction by removing the spectral image illuminated solely by ambient light. This eliminates the environmental illumination and improves the accuracy of subsequent analysis. **(2) Median Filtering and ROI Extraction.** To enhance the quality of the selected images, we employ median filtering to reduce noise. Additionally, for meat samples placed in circular petri dishes, we utilize the
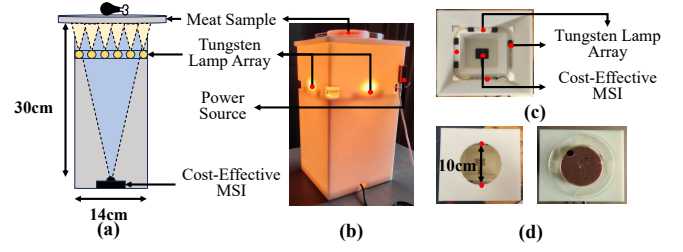

Figure 7: Prototype of MeatSpec, which cost <$60. Users can finish adulteration detection by simply placing the meat sample at the top of the box.

Hough Circle Transform [8] to extract the regions of interest (ROI). To achieve angle alignment of the extracted ROIs, we stick a black circular marker on each petri dish and rotate ROIs so that the marker centers are aligned. This approach compensates for variations in sample location and ensures accurate analysis. **(3) Spatial Alignment.** After cropping the images, we observe a resolution difference between the MSI and HSI images. To address this, we down-sample the larger image using nearest neighbor interpolation, ensuring they have the same size. Then by aligning the marker and meat centers along a vertical line, we eliminate misalignment and ensure accurate correspondence between MSI and HSI pairs. **(4) Central Area Extraction.** To focus on the most informative regions, we extract central areas of 320×320 pixels from the aligned MSI and HSI cubes. This enables efficient analysis and reduces computational complexity while preserving essential information for further processing.

Based on this pre-processing pipeline, we collect a spectral reconstruction dataset for minced beef adulteration inspection. Table 3 illustrates the adulteration types in our dataset. Based on the survey of various types of adulteration and their frequency in developing countries [28] and their harmfulness, we define six common types of adulteration. For each type of adulteration, we select several typical adulterants, resulting in a total of 13 different adulterants. Each adulterant is used at two concentrations, including a minimum adulteration concentration and a typical adulteration concentration [1]. The concentrations are set with reference to various surveys and standards [10, 18, 22]. We produce three samples for each adulterant and scan collect four (MSI, HSI) images for each sample. Overall, a total of 347 paired MSI and HSI images are collected, which can be accessed in [31].

4 IMPLEMENTATION

We implement a compact and low-cost prototype using off-the-shelf multispectral camera (named Monarch [44]) and

---

[1]For example, the "10%, 50%" indicates the 1:9 or 5:5 mass ratio of the adulterant to the beef. The "(0.75,3) ug/kg" means that the 0.75 ug/kg or 3 ug/kg concentration additives are prepared and sprayed on the surface of the beef sample.

Table 4: Comparing the parameters of the MSI and HSI cameras used in our experiment.

Parameters	Cubert (HSI)	Monarch (MSI)
Spectral Range	450-1000 nm	690-950nm
Spatial Size	1000×1000 pixels	1280×1024 pixels
Band Num	138	10
Wavelength (nm)	[450:1000::4] (*i.e.*, 450, 454, 458, 462, ..., 1000)	713, 736, 759, 782, 805, 828, 851, 874, 897, 920
Cost	>$10,000	≈$50

light components. As shown in Figure 7, the prototype is a semi-enclosed 3D printed box using white resin. The multi-spectral camera is placed at the bottom of the box with the lens facing up. Users can finish sample scanning by simply placing the meat sample at the top of the box. To capture one image, it takes about 750*ms*.

Multispectral Camera. Monarch has two advantages over other commercial multispectral cameras on the market that prompt us to choose it. First, most low-cost multispectral cameras on the market only cover visible light [39], but Monarch operates at frequencies ranging from 690*nm* to 950*nm* in the near-infrared band, providing more spectral features relevant to meat adulteration detection. Second, it's cheaper, Monarch uses the novel MEMS spectral imaging chip based on Fabry-Perot broadband filter to dramatically reduce the cost of hardware, which costs around $50 for mass production.

Light Source. We need to ensure sufficient light intensity at the sample to produce clear multispectral images. To this end, we place 12 full-band tungsten lamps (VCC7216-ND) at a distance of 10*cm* from the top of the box. All the lamps are connected in parallel and powered by a teensy@4.0 development board [37]. In addition, To ensure uniform illumination distribution, as shown in Figure 7 (c), the 12 lamps are uniformly placed at the the four walls of the box.

5 PERFORMANCE EVALUATION

5.1 Study Setup

5.1.1 Training Scheme. As mentioned in § 3.3, the paired HSI and MSI in our dataset both have 320×320 pixels after processing. To train the AOSR model, we split the images into 64×64 patches, with a batch size of 32, an initial learning rate of 10^{-4}, and a cosine preselection annealing decline to 10^{-6}. The model converges with a loss function weight (α) of 0.95 after 20000 iterations. To train the RAAD model, we use a batch size of 64, a distillation weight (β) of 0.8, an initial learning rate of 5×10^{-4}, and cosine preselection annealing with a rate of 10^{-6}. After training 1000 epochs, to prevent falling into a local optimum under cosine annealing, we reset the learning rate to a constant value of 5×10^{-5} and continue

training the model with additional 1000 epochs. The RAAD classification model converges to the final result after 2000 epochs.

5.1.2 Metrics. We reformulate the meat adulteration inspection task into a multi-classification task, which not only should distinguish the adulterated sample from the authentic sample but also detect the adulteration types. As depicted in § 3.3, we consider six common types of adulteration. Thus, we have 7 classes in total, including authentic beef (0), substitution (1), dye substitution (2), low-quality meat (3), edible additives (4), water injection (5), and toxic additives (6). To evaluate the performance of meat adulteration multi-classification task, we exploit the **Macro-averaging Accuracy** and **F1 score** as the metrics.

5.1.3 Baselines. We compare our system's performance with several baselines. *(i) RGB.* We use the corresponding RGB images generated by the captured HSI to conduct the classification. We build a ResNet [14] network to classify the generated RGB images. *(ii) MSI.* We directly use MSI images for classification. We use random forest, which is typically used in previous works [24], to classify the spectra that averaged in spatial dimension. *(iii) MSI (SOTA SR).* We use the existing SOTA spectral reconstruction algorithm [27] to reconstruct the HSI, and then use random forest to classify the average spectra in spatial dimension according to the conventional methods [24]. *(iv) HSI.* We use hyperspectral data collected by an expensive HSI camera [12] for classification, and use our designed CNN classifier. Tabel 4 shows more detailed parameters of the HSI camera comparing with our MSI camera. Note that although the performance of Meat-Spec is supposed to be inferior to this baseline, MeatSpec far outperforms this solution in terms of price.

5.2 Overall Performance

We first evaluate MeatSpec's performance on different adulteration type detection by conducting stratified 5-fold cross validation[2], by which the ratio between the target classes is the same in each fold as it is in the full dataset.

5.2.1 Baselines Comparison. Figure 8 compares the accuracy and F1-score of our MeatSpec with baselines, revealing three important findings. Firstly, using unmodified MSI or RGB for adulteration detection results in poor performance, with less than 70% accuracy, due to their limited and coarse-grained spectral information. Secondly, applying the existing SOTA SR algorithm to MSI only slightly improves the system's performance, since it fails to recover fine-grained differences and combat reconstruction errors in reconstructed HSI, leading to low classification accuracy. Finally, our designed system

---

[2]Doing stratified cross-validation can ensure that the cross-validation result is a close approximation of generalization error.
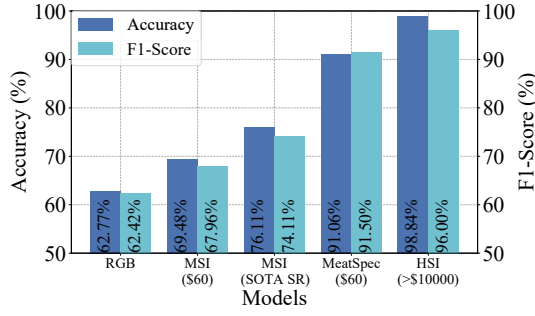
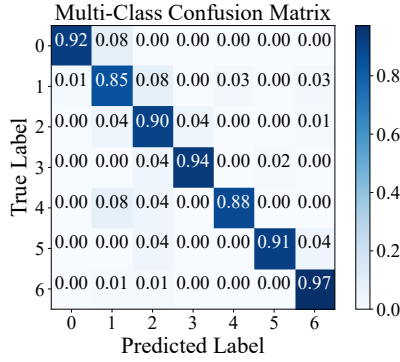**Figure 8: Stratified 5-fold cross-validation performance comparison between MeatSpec and baselines.**

Figure 9: Confusion matrix of MeatSpec on multiple meat adulteration types detection

achieves 91.06% accuracy for the meat adulteration type detection task, which is 21.58% higher than that of the direct use of MSI and 14.95% higher than that of the MSI using the existing reconstruction algorithm, demonstrating the effectiveness of the system design.

5.2.2 MeatSpec's Performance. Figure 9 and Figure 10 present the confusion matrix and AUC-ROC curve of MeatSpec for detecting multiple meat adulteration types, respectively. We can observe the consistently good performance of Meat-Spec across all adulteration types. Notably, MeatSpec can accurately distinguish authentic beef samples from adulterated samples, achieving an accuracy of 92%, even with various types of adulteration. Moreover, we conduct two-dimensional t-distributed stochastic neighbor embedding (t-SNE) projections [45] to illustrate the embedding representations of MeatSpec. Figure 11 displays our results, which indicate that MeatSpec displays clear clustering of all classes, demonstrating its aptitude for identifying various adulteration types.

5.3 Ablation Study

We then investigate the modules of MeatSpec by conducting ablation study to demonstrate the effectiveness of the system design.

5.3.1 Effectiveness of Application-oriented Spectral Reconstruction. From the results shown in Table 5, we can find that by introducing AOSR scheme, the system improves about 7.76% accuracy than the baseline, which indicates its effectiveness of gaining more spectral features related to adulteration types. Specifically, by involving adulteration prior information and contrastive loss, the distance between the selected sample and the samples of other adulteration classes is increased, thus helping the reconstruction model to learn the nuances between the adulteration samples of different classes.

5.3.2 Effectiveness of Reconstruction-adapted Adulteration Detection. The effectiveness of the RAAD structure is reflected in the results of Table 5, which show an accuracy improvement of 11.25% compared to the baseline. This structure enhances the model's recognition ability in two ways. Firstly, it extracts more information from the visible light band to compensate for the large reconstruction error of the reconstructed data. Secondly, by narrowing down the features of the HSI and reconstructed images, the model learns a feature space that is more similar to the HSI feature, thereby improving classification performance.

5.4 Impacts on Experimental Conditions

We then evaluate MeatSpec under various experimental and environmental conditions, as shown in Figure 12. We conduct the experiments using beef and one typical adulteration type, *i.e.*, substitute. For each experimental condition, we prepare two authentic samples and two substitute adulteration samples containing 50% of pork. Each sample is scanned by our prototype back and front twice, thus introducing eight authentic images and eight adulteration images. Both the reconstruction model and classification model are trained using all data collected in normal experimental conditions.

5.4.1 Varying Meat Size and Height. Our system is designed to be flexible, allowing users to vary the amount of meat used for detection, which can affect the size, shape, and thickness of the sample. To test our system's performance, we create samples of four sizes and five thicknesses. The results are shown in Figure 13(a)-13(b). We find that the system is more robust to different sizes than thicknesses. This is because our system eliminates the influence of ambient light by collecting a background map before scanning the sample. While the thickness of the sample can impact the system's performance, we find that our system performs well when the sample thickness is more than 1cm. Since beef patties on the market are generally 1-2cm thick, our system can handle most situations with ease.

5.4.2 Varying Meat Minced Size. The physical structure of minced beef with different degrees of grinding is different,
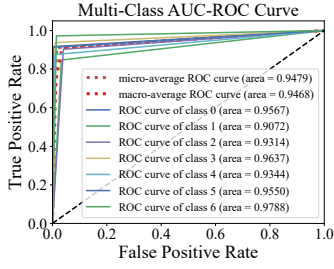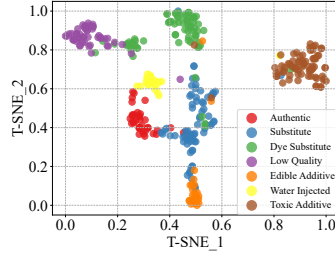
Figure 10: AUC-ROC Curve of MeatSpec's result.

Figure 11: T-SNE latent embedding distribution of Meat-Spec's classification model.

Ablation Models	Accuracy	F1-Score
MSI (SR)	76.11%	74.11%
MeatSpec (w/o RAAD)	83.87%	81.86%
MeatSpec (w/o AOSR)	87.36%	87.09%
MeatSpec (our)	**91.06%**	**91.50%**

Table 5: MeatSpec's performance comparing with ablation models and different base reconstruction models.

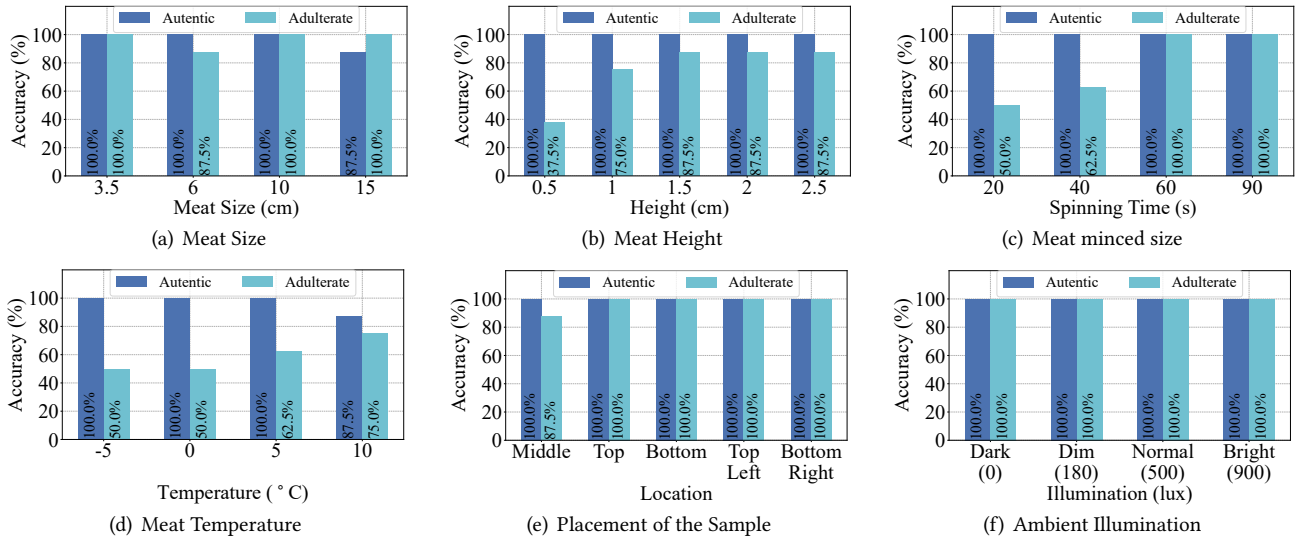**Figure 12: Illustration of various experimental conditions.**

Figure 13: MeatSpec performance under various experimental and environmental conditions.

which will affect the reflection and scattering route of light. Thus, we set the meat grinder to four different mixing times, which directly decide the degrees of grinding. As can be seen from Figure 13(c), when the stirring time is less than one minute, the performance of the system is affected, especially the performance of the production sample is significantly slightly reduced, which may be because the adulterants are not evenly mixed due to insufficient stirring. The spatial distribution of the collected MSI images is quite different from that of the fully mixed samples in the training set. This problem can be solved by calibration the model using coarse-particle samples. While, when the samples are fully mixed and grinding, the system can achieve good performance.

5.4.3 Varying Meat Temperature. The temperature of food affects its molecular thermal motions, which in turn affects the diffuse reflection of light. To evaluate MeatSpec under different food temperatures, we consider four common meat temperatures. The prepared samples are refrigerated at -18^oC for 8 hours and then thaw in normal temperature. Figure 13(d) reports the results, which indicate huge influence of temperature on our system. However, upon in-depth analysis of the classification results, we find that the misidentified samples are classified as either water-injected or low-quality substitution. This may be due to the precipitation of a lot of water in the process of refrigeration and thawing, and too long thawing time leads to the sample is not fresh.
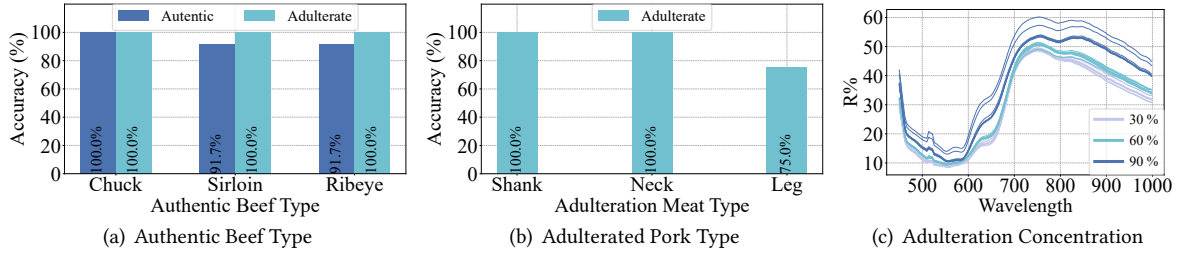
Figure 14: MeatSpec performance on generalization to various experimental setups.

5.4.4 Varying Sample Placement. Since our light source does not illuminate the sample uniformly from the center but from four sides, the meat samples may be exposed to different intensity light sources when placed at different scanning positions on the top. To test the robustness of the system to different positions, we use 6cm samples placed in five different areas on the top. The results in Figure 13(e) show that our system is not sensitive to the placement of the samples. This may be attributed to our background elimination algorithm and the classification model's pooling process, which eliminates the unevenness of the light field distribution

5.4.5 Varying Ambient Illumination. Ambient light can interfere with the readings of the MSI camera, which can negatively impact the performance of MeatSpec. Thus, we investigate the performance of MeatSpec under various realistic lighting conditions. We test the system under four different light settings. As shown in Figure 13(f), MeatSpec's performance is stable under different lighting conditions, as expected. This is because we place the camera at the bottom of the semi-closed box, blocking the majority of the ambient light, and utilize the proper background subtraction method.

5.4.6 Varying Authentic Beef Type. Minced beef on the market may be prepared using different types of beef. We select three representative beef parts, which are commonly used as raw materials for making ground beef [3]. We select a brand from a different origin for each part and calibrate the model using three parts of beef from one of the sources and then test it on samples from other sources. The results are shown in Figure 14(a). We can see that after calibration, the model also has good generalization performance for different parts of beef. If the users want to extend the model to more beef parts, only need to collect a small number of new parts of the sample to calibrate the model.

5.4.7 Varying Adulteration Meat Type. The same substitution class of adulteration may also include different kinds of substitutions, such as pork adulteration with different parts of pork. Therefore, taking pork adulteration as an example, we consider the adulteration of three different parts of pork. The model is also calibrated using a variety of pork parts,

---

[3]https://en.wikipedia.org/wiki/Ground_beef

and Figure 14(b) shows the results on the remaining samples. As shown in the Figure 14(b), except for leg pork, the model has a good prediction performance for different parts of adulterated pork, and leg pork is incorrectly classified as the alternative category of crying dye, which may be caused by the rich content of myoglobin in leg pork.

5.4.8 Varying Adulteration Concentration. We also experiment with adjusting the concentration of adulterants. Since different adulteration concentrations have a greater impact on sample composition, we mainly focus on whether the reconstructed spectra of adulterants with different contents could be effectively distinguished from each other. As shown in Figure 14(c), the average spectra of reconstructed hyperspectral images under three adulteration concentrations are presented. It is evident that as the adulteration concentration increases, the reflectance of the spectra becomes higher, and the spectra of samples with different adulteration concentrations can be easily distinguished from each other.

5.4.9 Multi-Type Adulteration. We further evaluate MeatSpec's performance in predicting multiple types of adulterants simultaneously. We include five two-type mixed cases and two three-type mixed cases commonly found in real scenarios. The label of mixed cases included 1-2, 1-3, 1-4, 2-3, 2-4, 1-2-3, and 1-2-4. Each case involves mixing different adulterated samples with 50% concentration and creating one sample to fine-tune the classification model and multiple samples for testing. The model, trained on a single-type dataset, achieved an 86.48% F1-Score, with a 68.85% exact match ratio for multi-label and a 92.39% accuracy for each instance. These results demonstrate MeatSpec's effectiveness in detecting multiple types of adulterants by distinguishing their unique spectral characteristics, thanks to MeatSpec's ability to restore fine-grained spectral information.

6 RELATED WORK

In this section, we briefly review existing works related to meat adulteration detection, hyperspectral reconstruction algorithms and cost-effective spectral systems.

Meat Adulteration Detection. Various methods have been developed for detecting meat adulteration, each with its own advantages and limitations [7, 52]. Early detection

methods [26, 33, 34, 36], offer accurate detection of animal DNA compositions in meat products but often involve complex sample preparation procedures. Electronic noses and spectroscopy techniques [20, 21, 25] are capable of obtaining accurate results without sample preparation but require expensive equipment. Smartphone-based solutions only rely on visual features [32, 38, 42, 43] thus may struggle to scale up to more harmful adulteration scenarios involving excessive additives. In contrast, MeatSpec uses a reconstruction algorithm to improve the spectral granularity of the system, thus significantly reducing the cost of the system and can identify more adulterants.

Hyperspectral Reconstruction Algorithms. The idea of hyperspectral reconstruction is to reconstruct full hyperspectral data from limited spectral measurements, reducing the need for expensive and bulky hardware components. Conventional spectral reconstruction methods rely on hand-crafted hyperspectral priors [3, 11, 29]. Recently, deep learning techniques have been applied to learn the mapping function from RGBs to HSIs [2, 27, 41, 49–51]. However, these algorithms always ignore the deployment of reconstructed spectra in practical applications. In the context of meat adulteration detection, by combining advanced spectral reconstruction algorithms with application-specific adjustments, MeatSpec provides a more tailored and effective solution for meat adulteration detection.

Cost-Effective Spectral System. Spectral systems are valuable for substance identification but expensive, which always cost $10,000, and inaccessible for many users. Researchers are working on making them more affordable and accessible. To address this, efforts have been made to simplify one-dimensional spectrometers using cheap LED and photodiode components [15–17, 30]. However, since lack of spatial-wise information, these systems can only work on liquid samples or homogeneous samples. Some systems use fewer components, sacrificing spectral resolution and requiring a large physical size [13]. There have also been efforts to use smartphones as spectral imaging systems, such as MobiSpectal [40], which focuses on the robustness of reconstructed spectra under different ambient light conditions. In contrast, MeatSpec operates in a semi-closed environment with minimal environmental interference, allowing it to focus on improving the quality of the reconstructed spectrum for fine-grained applications.

7 DISCUSSION

In this section, we will discuss the limitations and potential extensions of MeatSpec.

Unseen Adulterants and Concentration. MeatSpec focuses on beef adulteration and demonstrates high accuracy in detecting six common types of adulteration. However, due to the complexity of the adulteration issue, addressing all cases in one study is challenging. MeatSpec faces practical usage challenges with unseen cases. To address unseen concentration of known adulterants, the reconstruction model can be reused, but the classification model requires retraining with new targets. For a new adulteration type, fine-tuning the reconstruction model by incorporating a new loss function comparing the new type with others is necessary. Additionally, MeatSpec's detection capability is limited to surface-level adulterants due to the light's penetration depth. For instances of sub-surface adulteration, alternative detection methods should be explored.

Hardware Selection. Our paper expands the capability domain of low-cost spectral devices by using algorithms to distinguish samples with high similarity. If there is a similar performance but lower cost of multi-spectral hardware or better performance of spectral reconstruction algorithms, the framework of MeatSpec we designed can still be improved on alternative hardware and base reconstruction models.

Extension Applications. Furthermore, our proposed system has the potential to be used to solve other food adulteration problems, such as cereals and dairy products. By offering such a consumer solution for food adulteration detection, we can integrate these solutions into centralized dining settings to ensure the food safety of the users.

8 CONCLUDING REMARKS

This paper presents MeatSpec, a consumer-grade spectral imaging system for meat adulteration inspection. MeatSpec simultaneously guarantees the fine-grained spectral capability required for meat adulteration detection and maintains a low-cost hardware setup. To achieve this, MeatSpec utilizes the existing spectral reconstruction technology and incorporates two novel modules, namely AOSR and RAAD. AOSR involves adulteration-related prior information and contrastive learning to reconstruct more easily distinguishable full-band hyperspectral images. RADD devises a CNN-based adulteration detection model based on the error distribution characteristics of the reconstructed HSI, and enhanced by knowledge distillation structure. We also assemble an extensive dataset containing diverse adulterants. Experimental evaluations demonstrate that our system achieves a 91.06% accuracy in detecting multiple adulteration types, which surpasses the baseline performance without our proposed designs by 21.58%.

ACKNOWLEDGMENTS

REFERENCES

[1] Rabia Shabir Ahmad, Ali Imran, and Muhammad Bilal Hussain. 2018. Nutritional composition of meat. *Meat science and nutrition* 61, 10.5772 (2018), 61–75.

[2] Aitor Alvarez-Gila, Joost Van De Weijer, and Estibaliz Garrote. 2017. Adversarial networks for spatial context-aware spectral image reconstruction from RGB. In *Proceedings of the IEEE international conference on computer vision workshops*. 480–490.

[3] Boaz Arad and Ohad Ben-Shahar. 2016. Sparse recovery of hyperspectral signal from natural RGB images. In *Computer Vision–ECCV 2016: 14th European Conference, Amsterdam, The Netherlands, October 11–14, 2016, Proceedings, Part VII 14*. Springer, 19–34.

[4] Yuanhao Cai, Jing Lin, Zudi Lin, Haoqian Wang, Yulun Zhang, Hanspeter Pfister, Radu Timofte, and Luc Van Gool. 2022. Mst++: Multi-stage spectral-wise transformer for efficient spectral reconstruction. In *Proceedings of the IEEE/CVF Conference on Computer Vision and Pattern Recognition*. 745–755.

[5] The National Agricultural Law Center. 2023. The Adulterating Foodborne Pathogens: Meat, Poultry, and Some Egg Products. https://nationalaglawcenter.org/the-adulterating-foodborne-pathogens-meat-poultry-and-some-egg-products/.

[6] Qiuzhi Chang, Weike Wang, Gili Regev-Yochay, Marc Lipsitch, and William P Hanage. 2015. Antibiotics in agriculture and the risk to human health: how worried should we be? *Evolutionary applications* 8, 3 (2015), 240–247.

[7] Junhua Du, Mailin Gan, Zhongwei Xie, Chengpeng Zhou, Menglin Li, Meng Wang, Haodong Dai, Zhiyang Huang, Lei Chen, Ye Zhao, et al. 2023. Current progress on meat food authenticity detection methods. *Food Control* (2023), 109842.

[8] Richard O Duda and Peter E Hart. 1972. Use of the Hough transformation to detect lines and curves in pictures. *Commun. ACM* 15, 1 (1972), 11–15.

[9] Lemonia-Christina Fengou, Alexandra Lianou, Panagiotis Tsakanikas, Fady Mohareb, and George-John E Nychas. 2021. Detection of meat adulteration using spectroscopy-based sensors. *Foods* 10, 4 (2021), 861.

[10] Food and Agriculture Organization. 2022. FAOLEX Database. https://www.fao.org/faolex/results/details/fr/c/LEX-FAOC176367/.

[11] Ying Fu, Yongrong Zheng, Lin Zhang, and Hua Huang. 2018. Spectral reflectance recovery from a single RGB image. *IEEE Transactions on Computational Imaging* 4, 3 (2018), 382–394.

[12] Cubert GmbH. 2023. FIREFLEYE 185. https://www.cubert-hyperspectral.com/products/fireleye-185.

[13] Mayank Goel, Eric Whitmire, Alex Mariakakis, T Scott Saponas, Neel Joshi, Dan Morris, Brian Guenter, Marcel Gavriliu, Gaetano Borriello, and Shwetak N Patel. 2015. HyperCam: hyperspectral imaging for ubiquitous computing applications. In *Proceedings of the 2015 ACM International Joint Conference on Pervasive and Ubiquitous Computing*. 145–156.

[14] Kaiming He, Xiangyu Zhang, Shaoqing Ren, and Jian Sun. 2016. Deep residual learning for image recognition. In *Proceedings of the IEEE conference on computer vision and pattern recognition*. 770–778.

[15] Haiyan Hu, Qianyi Huang, and Qian Zhang. 2023. BabyNutri: A Cost-Effective Baby Food Macronutrients Analyzer Based on Spectral Reconstruction. *Proceedings of the ACM on Interactive, Mobile, Wearable and Ubiquitous Technologies* 7, 1 (2023), 1–30.

[16] Qianyi Huang, Zhice Yang, and Qian Zhang. 2018. Smart-U: smart utensils know what you eat. In *IEEE INFOCOM 2018-IEEE Conference on Computer Communications*. IEEE, 1439–1447.

[17] Yongzhi Huang, Kaixin Chen, Lu Wang, Yinying Dong, Qianyi Huang, and Kaishun Wu. 2021. Lili: liquor quality monitoring based on light signals. In *Proceedings of the 27th Annual International Conference on Mobile Computing and Networking*. 256–268.

[18] Zhongtao Huang, Bin Li, Shichang Wang, Rongguang Zhu, Xiaomin Cui, and Xuedong Yao. 2023. Robust and accurate classification of mutton adulteration under food additives effect based on multi-part depth fusion features and optimized support vector machine. *Food Analytical Methods* 16, 5 (2023), 933–946.

[19] Sang-Hee Jeong, Daejin Kang, Myung-Woon Lim, Chang Soo Kang, and Ha Jung Sung. 2010. Risk assessment of growth hormones and antimicrobial residues in meat. *Toxicological research* 26 (2010), 301–313.

[20] Hongzhe Jiang, Fengna Cheng, and Minghong Shi. 2020. Rapid identification and visualization of jowl meat adulteration in pork using hyperspectral imaging. *Foods* 9, 2 (2020), 154.

[21] Hongzhe Jiang, Wei Wang, Hong Zhuang, Seung-Chul Yoon, Yi Yang, and Xin Zhao. 2019. Hyperspectral imaging for a rapid detection and visualization of duck meat adulteration in beef. *Food Analytical Methods* 12 (2019), 2205–2215.

[22] Rongchang Jiang, Jingxin Shen, Xinran Li, Rui Gao, Qinghe Zhao, and Zhongbin Su. 2022. Detection and recognition of veterinary drug residues in beef using hyperspectral discrete wavelet transform and deep learning. *International Journal of Agricultural and Biological Engineering* 15, 1 (2022), 224–232.

[23] Mohammed Kamruzzaman, Yoshio Makino, and Seiichi Oshita. 2016. Rapid and non-destructive detection of chicken adulteration in minced beef using visible near-infrared hyperspectral imaging and machine learning. *Journal of Food Engineering* 170 (2016), 8–15.

[24] Zhilong Kang, Yuchen Zhao, Lei Chen, Yanju Guo, Qingshuang Mu, and Shenyi Wang. 2022. Advances in machine learning and hyperspectral imaging in the food supply chain. *Food Engineering Reviews* 14, 4 (2022), 596–616.

[25] Diclehan Karakaya, Oguzhan Ulucan, and Mehmet Turkan. 2020. Electronic nose and its applications: A survey. *International journal of Automation and Computing* 17, 2 (2020), 179–209.

[26] Rudolf M Lequin. 2005. Enzyme immunoassay (EIA)/enzyme-linked immunosorbent assay (ELISA). *Clinical chemistry* 51, 12 (2005), 2415–2418.

[27] Jiaojiao Li, Chaoxiong Wu, Rui Song, Yunsong Li, and Fei Liu. 2020. Adaptive weighted attention network with camera spectral sensitivity prior for spectral reconstruction from RGB images. In *Proceedings of the IEEE/CVF Conference on Computer Vision and Pattern Recognition Workshops*. 462–463.

[28] Xiaoman Li, Mingwu Zang, Dan Li, Kaihua Zhang, Zheqi Zhang, and Shouwei Wang. 2023. Meat food fraud risk in Chinese markets 2012–2021. *npj Science of Food* 7, 1 (2023), 12.

[29] Yuqi Li, Chong Wang, and Jieyu Zhao. 2017. Locally linear embedded sparse coding for spectral reconstruction from RGB images. *IEEE Signal Processing Letters* 25, 3 (2017), 363–367.

[30] Hidenori Matsui, Takahiro Hashizume, and Koji Yatani. 2018. All-light: An alcohol-sensing smart ice cube. *Proceedings of the ACM on interactive, mobile, wearable and ubiquitous technologies* 2, 3 (2018), 1–20.

[31] MeatSpec. 2024. MeatSpec Meat Adulteration Spectral Reconstruction Dataset. https://drive.google.com/drive/folders/1mK7H9SZqEMkgJT3fQiuVL2PQwpw85r2m?usp=drive_link.

[32] Judith Müller-Maatsch and Saskia M van Ruth. 2021. Handheld devices for food authentication and their applications: A review. *Foods* 10, 12 (2021), 2901.

[33] Katarzyna Nalazek-Rudnicka, Ilona Kłosowska-Chomiczewska, Andrzej Wasik, and Adam Macierzanka. 2019. MRM–MS of marker peptides and their abundance as a tool for authentication of meat species and meat cuts in single-cut meat products. *Food chemistry* 283 (2019), 367–374.

[34] Tsugunori Notomi, Hiroto Okayama, Harumi Masubuchi, Toshihiro Yonekawa, Keiko Watanabe, Nobuyuki Amino, and Tetsu Hase. 2000. Loop-mediated isothermal amplification of DNA. *Nucleic acids research* 28, 12 (2000), e63–e63.

[35] World Health Organization. 2022. Food safety. https://www.who.int/news-room/fact-sheets/detail/food-safety.

[36] Adrian Pickar-Oliver and Charles A Gersbach. 2019. The next generation of CRISPR–Cas technologies and applications. *Nature reviews Molecular cell biology* 20, 8 (2019), 490–507.

[37] PJRC. 2022. teensy40. https://www.pjrc.com/store/teensy40.html.

[38] Narjiss Seddaoui and Aziz Amine. 2021. Smartphone-based competitive immunoassay for quantitative on-site detection of meat adulteration. *Talanta* 230 (2021), 122346.

[39] SEETRUM. 2024. SEETRUM. https://www.seetrum.com/.

[40] Neha Sharma, Muhammad Shahzaib Waseem, Shahrzad Mirzaei, and Mohamed Hefeeda. 2023. MobiSpectral: Hyperspectral Imaging on Mobile Devices. In *Proceedings of the 29th Annual International Conference on Mobile Computing and Networking*. 1–15.

[41] Zhan Shi, Chang Chen, Zhiwei Xiong, Dong Liu, and Feng Wu. 2018. Hscnn+: Advanced cnn-based hyperspectral recovery from rgb images. In *Proceedings of the IEEE Conference on Computer Vision and Pattern Recognition Workshops*. 939–947.

[42] Weiran Song, Nanfeng Jiang, Hui Wang, and Jordan Vincent. 2020. Use of smartphone videos and pattern recognition for food authentication. *Sensors and Actuators B: Chemical* 304 (2020), 127247.

[43] Weiran Song, Yong-Huan Yun, Hui Wang, Zongyu Hou, and Zhe Wang. 2021. Smartphone detection of minced beef adulteration. *Microchemical Journal* 164 (2021), 106088.

[44] Unispectral. 2023. Unispectral Monarch. https://www.unispectral.com/product/monarch-nir-pcb/.

[45] Laurens Van der Maaten and Geoffrey Hinton. 2008. Visualizing data using t-SNE. *Journal of machine learning research* 9, 11 (2008).

[46] Saskia M van Ruth and Onno Nillesen. 2021. Which company characteristics make a food business at risk for food fraud? *Foods* 10, 4 (2021), 842.

[47] Wenbo Wang and Jitendra Paliwal. 2007. Near-infrared spectroscopy and imaging in food quality and safety. *Sensing and instrumentation for food quality and safety* 1 (2007), 193–207.

[48] Amanda Watson, Claire Kendell, Anush Lingamoorthy, Insup Lee, and James Weimer. 2023. Lumos: An Open-Source Device for Wearable Spectroscopy Research. *Proceedings of the ACM on Interactive, Mobile, Wearable and Ubiquitous Technologies* 6, 4 (2023), 1–24.

[49] Zhiwei Xiong, Zhan Shi, Huiqun Li, Lizhi Wang, Dong Liu, and Feng Wu. 2017. Hscnn: Cnn-based hyperspectral image recovery from spectrally undersampled projections. In *Proceedings of the IEEE International Conference on Computer Vision Workshops*. 518–525.

[50] Yiqi Yan, Lei Zhang, Jun Li, Wei Wei, and Yanning Zhang. 2018. Accurate spectral super-resolution from single RGB image using multi-scale CNN. In *Pattern Recognition and Computer Vision: First Chinese Conference, PRCV 2018, Guangzhou, China, November 23-26, 2018, Proceedings, Part II 1*. Springer, 206–217.

[51] Yuzhi Zhao, Lai-Man Po, Qiong Yan, Wei Liu, and Tingyu Lin. 2020. Hierarchical regression network for spectral reconstruction from RGB images. In *Proceedings of the IEEE/CVF Conference on Computer Vision and Pattern Recognition Workshops*. 422–423.

[52] Qamar Zia, Mohammad Alawami, Nur Fadhilah Khairil Mokhtar, Raja Mohd Hafidz Raja Nhari, and Irwan Hanish. 2020. Current analytical methods for porcine identification in meat and meat products. *Food chemistry* 324 (2020), 126664.